Desalination and Water Treatment
www.deswater.com

doi: 10.1080/19443994.2015.1074118

57 (2016) 16034–16052
July

Taylor & Francis
Taylor & Francis Group

Application of activated carbon produced from phosphoric acid-based chemical activation of oil fly ash for the removal of some charged aqueous phase dyes: role of surface charge, adsorption kinetics, and modeling

B.A. Labaran, M.S. Vohra*

Civil and Environmental Engineering Department, King Fahd University of Petroleum & Minerals (KFUPM), P.O. Box 1196, Dhahran 31261, Kingdom of Saudi Arabia, Tel. +966 013 860 2854; Fax: +966 013 860 2879; emails: baljega@kfupm.edu.sa (B.A. Labaran), vohra@kfupm.edu.sa (M.S. Vohra)

Received 8 December 2014; Accepted 12 July 2015

ABSTRACT

Oil fly ash (OFA) waste from electric power plants poses a serious management challenge. To address this problem, we studied the conversion of OFA into activated carbon (AC) and investigated the application of the produced AC for the removal of several aqueous phase dyes. The latter investigation included a study of the effects of various process parameters, such as pH, AC amount, and initial dye concentration, on the efficiency of AC adsorption. The highest specific surface area (SSA_{BET}) value of 63 m^2/g was achieved for the produced AC sample using a phosphoric acid strength of 40% (w/w %), an impregnation ratio *R* of 0.8 (mL-acid/gm-fly ash), and a furnace temperature of 500˚C (for 2 h). Increased methylene blue (MB) adsorption onto AC was observed when the pH was above 5. At higher pH, the presence of positive amino groups on MB was indicated to favor its adsorption onto AC, which was found to have a dominant negative surface charge at pH values above 5.6 (i.e. pH_{zpc}). Furthermore, speciation of the AC surface functional groups, including O–H groups, was also invoked to explain the pH-dependent adsorption of MB onto OFA-based AC. In addition, methyl orange (MO) dye showed higher adsorption at acidic pH values, and an increase in pH from 2 to 8 caused a decrease in its adsorption, which was also attributed to its AC's of 5.6. The kinetics studies showed that the adsorption rate values are higher at lower dye concentrations. A better fit was observed for the second-order kinetics compared to the first-order kinetics. The Freundlich isotherm model provided a better fit for the adsorption of MB and MO, whereas the Langmuir model provided a better fit for rhodamine B (RB) adsorption. Furthermore, the response surface methodology (RSM)-based models also showed that the RSM approach can be used to predict the removal of RB, MB, and MO dyes from the aqueous phase using OFA-based AC under a varying set of operational conditions. In summary, the results from the present investigation indicate that OFA-based AC can be successfully used for the removal of several dye contaminants from wastewater streams by carefully optimizing the process conditions described in this work.

Keywords: Oil fly ash; Rhodamine B; Methyl orange; Methylene blue; Activated carbon; Adsorption

*Corresponding author.

1. Introduction

Electric power plants using heavy oil as an energy source produce large amounts of oil fly ash (OFA) as a waste material. Because it is difficult to handle and dispose of OFA waste, a sound and professional solution to this challenge, other than a simple disposal practice, is urgently needed. In this regard, the conversion of OFA into activated carbon (AC) offers the dual advantage of being an environmentally sound OFA waste handling solution that eventually produces a product that can be used for a variety of pollution control applications. This approach will also reduce the burden on the receiving landfills and the consequent negative environmental impacts, which in turn minimizes the community concerns related to the disposal and health effects of such waste material. Furthermore, several dyes and their degradation products are toxic and carcinogenic and must thus be treated before being discharged into the receiving water bodies [1]. For example, in the early 1990s, the annual textile-based usage of dyes was approximately 7,00,000 tons [2], whereas the global dye and pigment market is projected to grow further and reach 9 million tons by 2015 [3,4] because of increasing use in the textile industry. Therefore, the treatment of the increasing amount of dye effluent is an important issue. Several studies have reported the use of AC for the adsorption-based removal of dyes from contaminated wastewater streams [5–12]. Nevertheless, reports on the use of OFA-based AC for the removal of methylene blue (MB) are limited [8–12], and to the best of our knowledge, the application of OFA-based AC produced using a phosphoric acid-based chemical activation process for the removal of aqueous phase dyes including rhodamine B (RB) and methyl orange (MO) has not been reported. Hence, considering the above-mentioned concerns related to the disposal of OFA waste and the appropriate treatment of dye-contaminated wastewater streams, the present study investigated the production of AC from OFA. We also investigated the application of the produced AC for the removal of several aqueous phase dyes, along with the effect of various process parameters, such as pH, AC added, and initial dye concentration, on the efficiency of dye removal using OFA-based AC as an adsorbent. We also investigated the process kinetics and reported the adsorption models, including the response surface methodology (RSM) using Box–Behnken design (BBD) method-based models, to predict the adsorption efficiency under the above-mentioned process conditions. Although BBD employs fewer experiments, it is considered comparable to central composite designs and three-level full factorial designs that employ larger numbers of experiments [13]. Hopefully, the details as reported in the following sections will be of use in resolving the environmental issues and concerns.

2. Materials and methods

2.1. Chemicals

All chemicals used were of high-purity reagent grade quality. The major chemicals included RB (FISHER), MO (BDH), MB (FISHER), pH calibration standards (FISHER), phosphoric acid/KH_2PO_4 (BAKER), $HClO_4$ (BAKER), NaOH (FISHER), ethanol (Hayman), nitrogen gas (99.999%), helium gas (99.999%), and high-purity liquid nitrogen (at 77 K).

2.2. Adsorption experiments

2.2.1. Production of AC

Fig. 1 is a flow diagram of the various steps involved in the AC production process. The OFA sample was first thoroughly washed several times and then dried in an air oven at 120°C for 24 h. Next, in the impregnation step, a known amount of this OFA was mixed with predetermined volumes of phosphoric acid with varying concentrations of 40, 50, and 60% and kept in the oven overnight at 120°C. The amount of acid was adjusted to obtain the desired acid-to-OFA ratio (i.e. the impregnation ratio or ml-acid/gm-OFA). This impregnation step was then followed by the activation step for the preparation of AC, during which the slurry was transferred into stainless steel tubes with a diameter of 50 mm and length of 300 mm (including two narrow ports with a diameter of 8 mm to expel the gases). The tubes containing the slurry were kept inside a muffle furnace and heated at a slow rate to allow for the free evolution of volatiles at temperatures of 300–600°C. The time to withdraw the samples from the furnace was calculated from the time the furnace reached the final temperature. Subsequently, the cooled mass from the tubes was subjected to thorough washing with hot water until the washings show pH ≈ 7.0, and the washed sample was again dried in the oven at 120°C. We then determined the specific surface area (SSA_{BET}), pore volume, and average pore size for the samples. The SSA_{BET} for the prepared AC sample was obtained using classical BET theory and nitrogen adsorption isotherm data. A physisorption setup (Micromeritics ASAP 2020, USA) was used to obtain the nitrogen adsorption isotherm data, which were eventually used to determine the SSA_{BET}, micropore volume, and

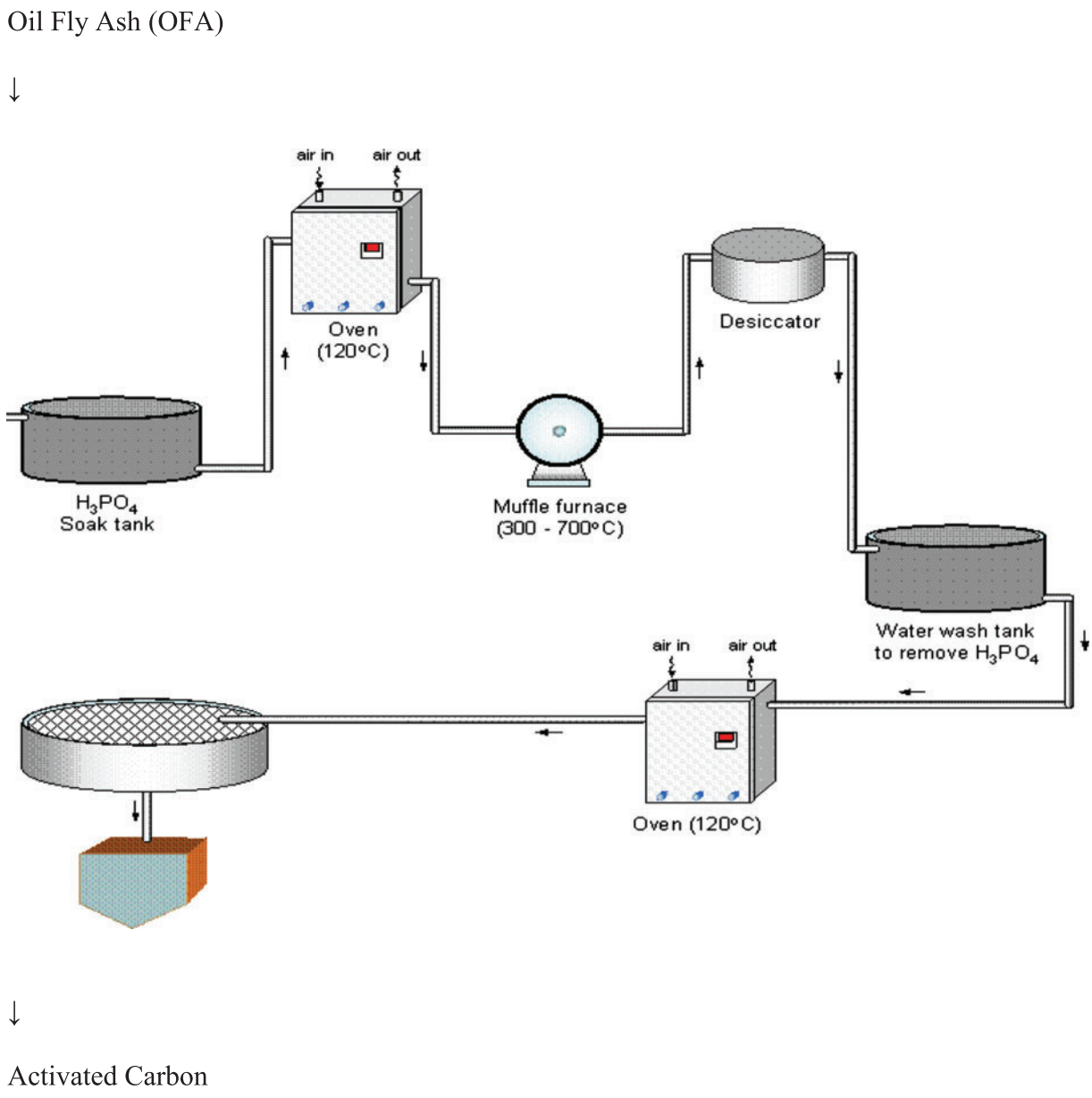

Fig. 1. Process flow diagram for the production of AC produced using phosphoric acid-based chemical activation of heavy OFA waste.

average pore width (4 V/A by BET) for the prepared AC samples.

2.2.2. *Effect of pH experiments*

The pH-based adsorption isotherm experiments were completed using 100-ppm dye. The test solutions were prepared using high-purity water (CORNING Mega Pure™ System) and appropriate volumes of already-prepared 1,000-ppm stock solutions of the dyes. For each dye, a batch of bottles with pH values between 2 and 12 was arranged. The suspensions were continuously mixed and samples were collected at various time intervals until equilibrium (in terms of the solution dye concentration) was reached. That dye concentration, along with the equilibrium pH, was used to obtain the pH–adsorption profile. The equilibrium pH data can be used to assess the optimum pH for the maximum removal of dye from the aqueous phase using the produced AC sample, which can

further be used for real-life applications, as the pH of wastewater stream will be adjusted to optimize its adsorption-based treatment.

2.2.3. Adsorption isotherm experiments

Adsorption isotherm experiments were also completed using 100-ppm dye. For each dye solution, a batch of bottles with AC dosages between 0 and 3,500 mg/L were arranged. The optimum pH obtained from the previous set of experiments was used for each dye adsorption isotherm study. The dye concentrations were monitored until the equilibrium concentration was reached. The equilibrium concentrations and AC dosages were noted for each dye, and the data were fitted to Freundlich and Langmuir adsorption isotherm models using the conventional procedures.

2.2.4. Adsorption kinetics experiments

The adsorption kinetics experiments were conducted with 1,000-ml test solutions using Pyrex glass bottles. The test solutions were prepared using high-purity water (CORNING Mega Pure™ System) and an appropriate volume of the already-prepared 1,000-ppm stock solutions of the dyes prepared using reagent grade chemicals. Base experiments with 10, 30, 50, and 200 ppm of dye were completed using 2-g/L AC at the optimum pH for each of the three dyes (RB, MB, and MO) obtained from the pH-based adsorption experiments. A blank sample was taken before the addition of the required amount of AC, followed by the adjustment of the pH to the desired value using HCl or NaOH solutions. The test solution was then kept in suspension using the standard stirring setup. Samples were withdrawn at different time intervals and then analyzed.

2.3. Analytical methods

2.3.1. Techniques used to analyze the surface properties

The % (w/w) carbon content of the AC produced from OFA was analyzed using a carbon analyzer (AnalytikJena Multi EX 2000, Germany). Furthermore, the SSA_{BET} value for the prepared AC sample was obtained via classical BET theory and nitrogen adsorption isotherm data. A physisorption setup (Micromeritics ASAP 2020, USA) was used to obtain the nitrogen adsorption isotherm data that were eventually used to determine the SSA_{BET}, *t*-plot micropore volume, and average pore width (4 V/A by BET) for the prepared AC. The Fourier transform infrared (FTIR) spectra for the produced AC in the 4,000–400 cm^{-1} region were obtained using a standard FTIR setup (6700 Nicolet FTIR unit, Thermo Scientific, USA) and KBr pellet technique. The thermogravimetric analysis (TGA) of OFA-based AC was completed using a standard TGA analyzer (TGA 4000, Perkin Elmer, USA). High-purity nitrogen gas was also used during the TGA analyses. The zero-point charge value (pH_{zpc}) for the AC sample that was used for all adsorption studies was determined with ZETATRAC equipment (MICROTRAC INC., USA).

2.3.2. Techniques used to analyze the water samples

Each sample was first filtered using a filter with 0.2-μm pores (Whatman, Germany) and then analyzed in terms of the pollutant levels. For example, the MB analyses were completed using a UV–vis spectrophotometer system (Shimadzu, Japan). For each individual experiment, a separate set of calibration standards was prepared using the blank sample that was collected after adjusting the pH during each experiment. This pH adjustment was performed to ensure that the standards and analytes of interest were at the same pH value. For each analysis, the sample was transferred into a clean cuvette, and the absorption value at a wavelength of 663 nm was noted for further processing using standard procedures. The UV–vis spectrophotometer system was calibrated using MB standards. Similar procedures were adopted for RB and MO at wavelengths of 599 and 465 nm, respectively. All pieces of equipment and analyzers were regularly calibrated before each analysis exercise using the calibration standards. The pH analyses were conducted using a standard pH electrode-meter setup (AccuTupH$^+$ 13-620-185 electrode, Accumet XL15 pH meter), which was also regularly calibrated using pH calibration standards.

2.4. RSM modeling

For RSM modeling, the BBD method was employed for the experimental design and analysis. Three independent variables—pH, initial dye concentration, and AC dosage—were used for each of the three dyes. In addition, three equally spaced levels were adopted for each of the variables: pH (4, 7, and 10), initial dye concentration (50, 100, and 150 ppm), and AC dosage (1,000, 1,500, and 2,000 mg/L). With a single center point per block, the design produced 13 experiments for each dye. The responses (percent adsorption) obtained from the experiments were

analyzed using the Design-Expert software with a one-way analysis of variance.

3. Results and discussion

3.1. Selective surface properties

OFA-based AC was first produced using the chemical activation method (details given in Section 2). The highest SSA_{BET} value was achieved for a phosphoric acid strength of 40% (w/w %), an impregnation ratio R of 0.8 (mL-acid/gm-fly ash), and a furnace temperature of 500°C (for 2 h). Fig. 2a provides the BET adsorption isotherms and Table 1 summarizes several physical–chemical properties of the produced AC. The SSA_{BET} value is equal to 63 m^2/g. The t-plot micropore volume is 0.02 cm^3/g. In addition, the average pore width of the produced AC is ca. 46.08 Å (using 4 V/A by BET). According to the IUPAC pore size classification, this pore width indicates the mesoporous nature of the produced AC. The % (w/w) carbon content of the produced AC was analyzed and found to be equal to 68%. The initial OFA (raw) contained 62% carbon and minor amounts of silica, alumina, magnesium, and sulfur. Furthermore, the chemical activation of OFA also introduces various surface functional groups, which provide the surface sites for adsorption. The AC surface functional groups, including O-based surface species, such as O–H, contribute to the removal of the target pollutant. To explore such functional groups on the produced AC surface, an FTIR analysis was also conducted, and the results are given in Fig. 2b. For example, the band at 3,428 cm^{-1} indicates the presence of O–H stretching vibration. The zero-point charge value (pH_{zpc}) for the AC sample was also determined, and results are given in Fig. 2c. The pH_{zpc} value is approximately 5.6; thus, below pH 5.6, the produced AC surface will be dominantly positive, whereas at pH values above 5.6, the produced AC surface will have an overall negative surface charge. Such changes in surface charge will tend to affect the adsorption of target pollutants, particularly aqueous phase contaminants (e.g. dyes) that show a pH-dependent speciation. This issue is discussed in detail in Section 3.2. Furthermore, the TGA analysis results for both the OFA and produced AC are presented in Fig. 2d. For the OFA, a gradual weight loss of approximately 35% is noted until 700°C. These trends indicate an initial water loss phase followed by hydrocarbon losses. However, the produced AC shows no significant change in weight, which can be attributed to the loss of volatiles during the activation process (Fig. 2d). All adsorption experiments reported in this study were completed using the same AC sample without any further treatment.

3.2. Effect of pH

Speciation of both the adsorbate and adsorbent affects the interaction between the two and thus affects the overall adsorption efficiency. Hence, the

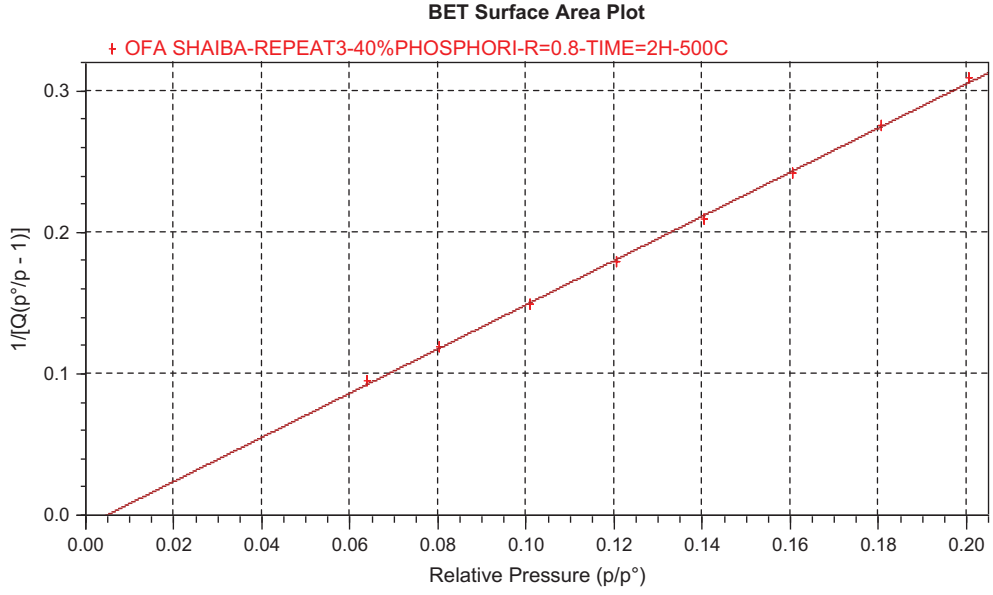

Fig. 2a. BET specific surface area plot for AC produced using OFA waste employing 40% (w/w) phosphoric acid as an activation agent at an impregnation ratio R = 0.8 (v-acid/w-OFA), 500°C furnace temperature, and duration of 2 h.

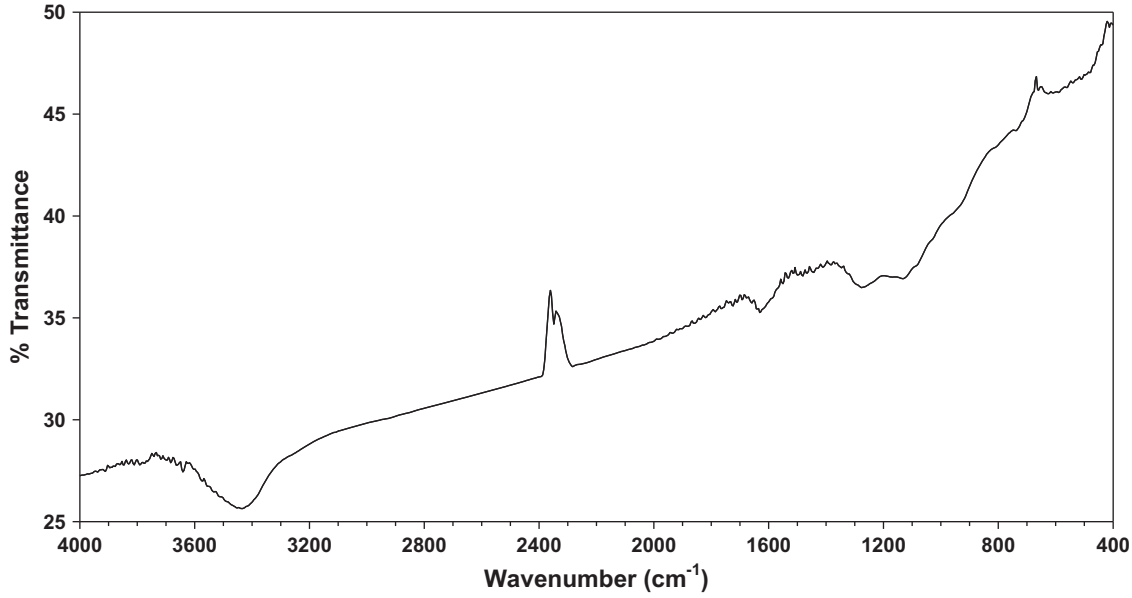

Fig. 2b. FTIR spectra of AC produced using OFA waste employing 40% (w/w) phosphoric acid as an activation agent at an impregnation ratio R = 0.8 (v-acid/w-OFA), 500˚C furnace temperature, and duration of 2 h.

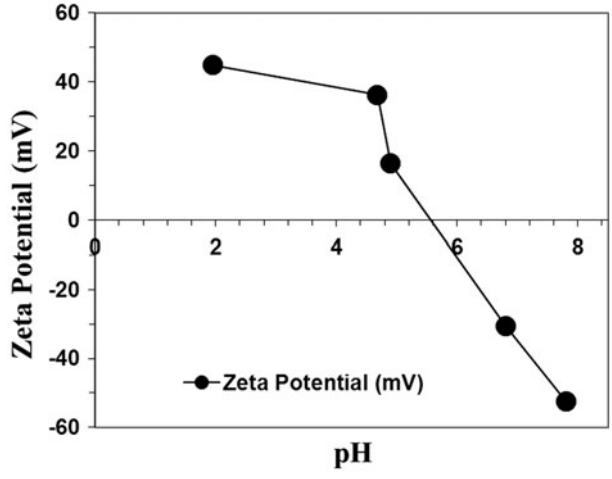

Fig. 2c. Effect of pH on zeta potential for AC produced using OFA waste employing 40% (w/w) phosphoric acid as an activation agent at an impregnation ratio R = 0.8 (v-acid/w-OFA), 500˚C furnace temperature, and duration of 2 h.

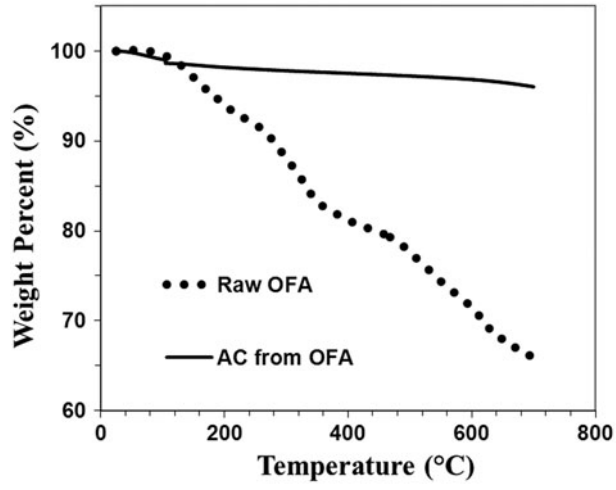

Fig. 2d. TGA results for OFA and also for AC produced using OFA waste employing 40% (w/w) phosphoric acid as an activation agent at an impregnation ratio R = 0.8 (v-acid/w-OFA), 500˚C furnace temperature, and duration of 2 h.

effect of pH on the adsorption of 100-ppm RB, MB, and MO onto 2 g/L of produced AC was first investigated. The effects of the pH on the adsorption of RB, MB, and MO onto the produced AC are shown in Figs. 3a–3d. The maximum adsorption of 75.5% occurs for RB at pH 4 (Fig. 3a). An increase in pH above 4 results in decreased adsorption, with the same trend noted until pH 12. A similar trend was observed by Guo et al. for the removal of RB onto rice husk-based porous carbon [14]. Fig. 2c shows the surface charge results for the AC used in this research. The pH_{zpc} value is approximately 5.6, and hence, below pH 5.6, the produced AC surface will be dominantly positive, whereas at pH values above 5.6, the produced AC surface will have an overall negative surface charge. Such changes in surface charge will tend to affect the

Table 1
Some physico-chemical properties of AC produced from OFA from Saudi electric power plant using 40% (w/w) phosphoric acid and an impregnation ration, $R = 0.8$ (v/w) at 500°C furnace temperature for 2 h

Property	Value
SSA_{BET}	63 m^2/g
t-plot micropore volume	0.02 cm^3/g
Average pore width [(4 V/A) by BET)]	46.08 Å
Carbon content (w/w)	68%

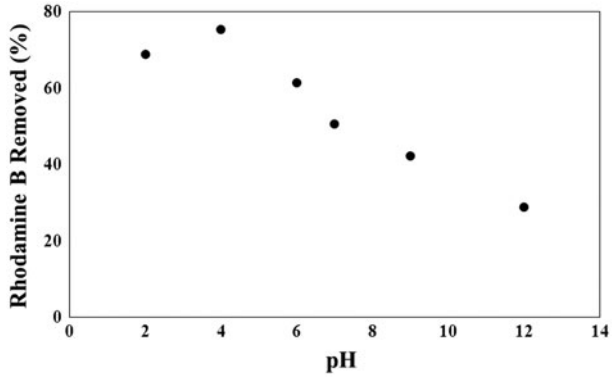

Fig. 3a. Effect of pH on the removal of rhodamine B from synthetic wastewater using 2-g/L AC produced using phosphoric acid-based chemical activation of OFA waste (rhodamine B = 100 ppm; AC dosage = 2 g/L).

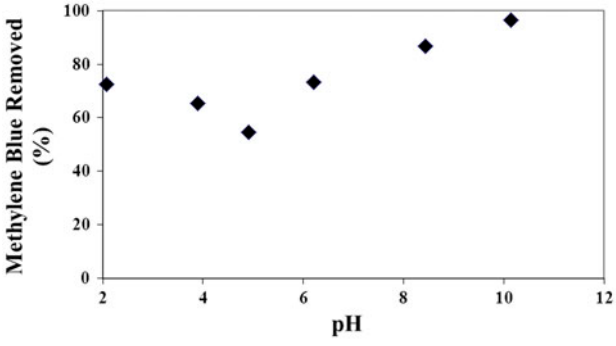

Fig. 3b. Effect of pH on the removal of MB from synthetic wastewater using 2-g/L AC produced using phosphoric acid-based chemical activation of OFA waste (MB = 100 ppm; AC dosage = 2 g/L).

adsorption of target pollutants, particularly aqueous phase contaminants (e.g. dyes) that show a pH-dependent speciation. For example, RB dye exists in cationic form below pH 4 and in zwitterionic form above pH 4 [14]. Hence, the optimum adsorption of RB onto AC

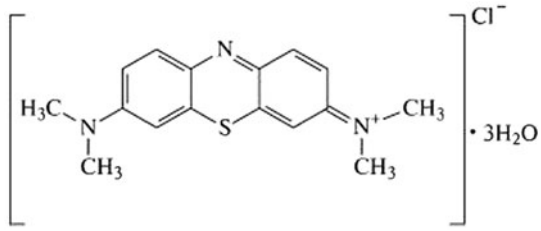

Fig. 3c. The molecular structure of a MB molecule.

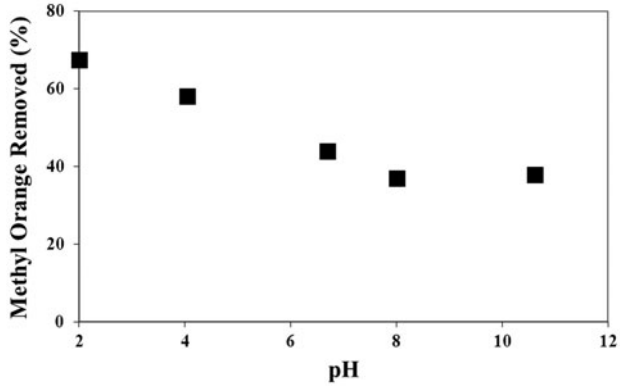

Fig. 3d. Effect of pH on the removal of MO from synthetic wastewater using 2-g/L AC produced using phosphoric acid-based chemical activation of OFA waste (MO = 100 ppm; AC dosage = 2 g/L).

was observed at pH 4 (Fig. 3a). However, a further increase in pH results in decreased RB adsorption because of an increased electrostatic repulsion between the dissociated carboxyl group on RB and the negatively charged AC surface with pH. Fig. 3b shows the effect of pH on the adsorption-based removal of MB using the produced AC. The maximum adsorption is observed at pH 10. A decrease in the adsorption of MB is noted as the pH is increased from 2 to 5, with the decrease being more noticeable between pH 4 and 5. However, increased MB adsorption is observed when the pH is further increased from 5 to 10. Similar to the RB results, electrostatic interactions between the cationic dye and charged AC surface alone cannot explain the noted trends (Fig. 3b). Fig. 3c shows the molecular structure of MB. Liu et al., who studied the dissociation of MB's functional groups [15], reported a dissociation constant of 8.5 for the amino group. Hence, at higher pH, the presence of positive amino groups favors its adsorption onto AC, which is dominantly negative at pH values above 5.6. Furthermore, the presence of AC surface functional groups, such as O–H groups (see Section 3.1 for details) is also used to

explain the pH-dependent adsorption of MB onto the produced AC. Hence, the pH-dependent adsorption of cationic MB onto the produced AC may be due to changes in the surface charge of AC and the speciation of MB with pH.

We also studied the adsorption of MO onto the produced AC, and the results are shown in Fig. 3d. The maximum MO removal is observed at pH 2. An increase in pH from 2 to 8 causes a nearly linear decrease in the adsorption of MO from approximately 67 to 37%. However, no significant change in MO adsorption is observed above pH 8. Furthermore, MO dye, which is anionic because of the presence of sulfonate groups, will be more efficiently removed from the aqueous phase with a cationic surface. Therefore, as also shown in Fig. 3d, higher MO adsorption occurs in the acidic pH range because of an electrostatic attraction between the anionic MO and cationic AC surface at lower pH, however, an increased negative charge on the AC surface at higher pH (Fig. 2c causes electrostatic repulsion between MO and the AC surface, thus resulting in decreased MO adsorption with pH (Fig. 3d). Significant dye adsorption could be achieved using a small amount of OFA-based AC with an appropriate adjustment of the process pH.

3.3. Adsorption kinetics

Adsorption kinetics plays an important role, specifically from the reactor design perspective [16] and considering that we first investigated the details under a varying set of conditions using a 1,000-mL test solution for each experiment. The adsorption kinetics of the dyes on the produced AC was studied at four different concentrations of RB, MB, and MO. The first- and second-order rate constants were determined by fitting the data to first- and second-order rate kinetic models, respectively. The findings are summarized in Table 2 and are also given in Figs. 4a–4c. A first-order rate constant of 0.5025 min^{-1} was obtained for the adsorption of 10-ppm RB onto AC (Table 2). The rate constant decreased to 0.0280 min^{-1} when the concentration was increased to 30 ppm (Table 2). A further decrease in the reaction rate constant to 0.0022 min^{-1} was observed when the concentration was further increased to 50 ppm. The lowest reaction rate constant of 0.0004 min^{-1} was noted for the adsorption of 200-ppm RB. This finding was further verified by comparing the adsorption of 50-ppm RB onto different dosages of AC. An increase in AC dosage from 1.5 to 2.0 g/L increases the reaction rate constant from 0.0017 to 0.0022 min^{-1}. An increase in the AC dosage from 1.5 to 2.0 g/L reduces the dye-to-adsorbent ratio and thus limits the saturation of higher energy sites. Second-order kinetic plots for the adsorption of different concentrations of RB onto 2.0-g/L AC are also shown in Fig. 4a. Second-order rate constants of 1.9794, 0.1468, 0.0005, and 6×10^{-6} L/mg min were obtained for the adsorption of 10, 30, 50, and 200-ppm RB onto 2.0-g/L AC, respectively. Similar to the first-order rate constants, an increase in the reaction rate constant was observed with a decrease in dye concentration. Furthermore, an increase in the reaction rate constant was also observed with an increase in AC dosage from 1.5 to 2.0 g/L. In addition, the first-order reaction rate constants for the adsorption of 10, 30, 50, and 200-ppm MB onto AC are given in Table 2. The minimum and

Table 2
Effect of initial dye concentration on to its adsorption rate constant for AC produced from phosphoric acid-based chemical activation of OFA waste (dye concentration = 10–200 ppm, AC amount 2 g/L)

		First-order		Second-order	
Dye type	Dye concentration (ppm)	Rate constant (min^{-1})	R^2	Rate constant (L/mg min)	R^2
Methylene blue	10	0.5661	0.7558	0.9124	0.766
	30	0.0130	0.7674	0.0183	0.9809
	50	0.0045	0.8293	0.0054	0.9848
	200	0.0001	0.9324	1×10^{-6}	0.9337
Rhodamine B	10	0.5025	0.8134	1.9794	0.8887
	30	0.0280	0.9115	0.1468	0.9974
	50	0.0022	0.8957	0.0005	0.9507
	200	0.0004	0.9953	6×10^{-6}	0.9949
Methyl orange	10	0.1542	0.9014	1.4801	0.9860
	30	0.0194	0.9835	0.0073	0.9996
	50	0.0016	0.9125	0.0002	0.9589
	200	0.0009	0.9976	3×10^{-5}	0.9928

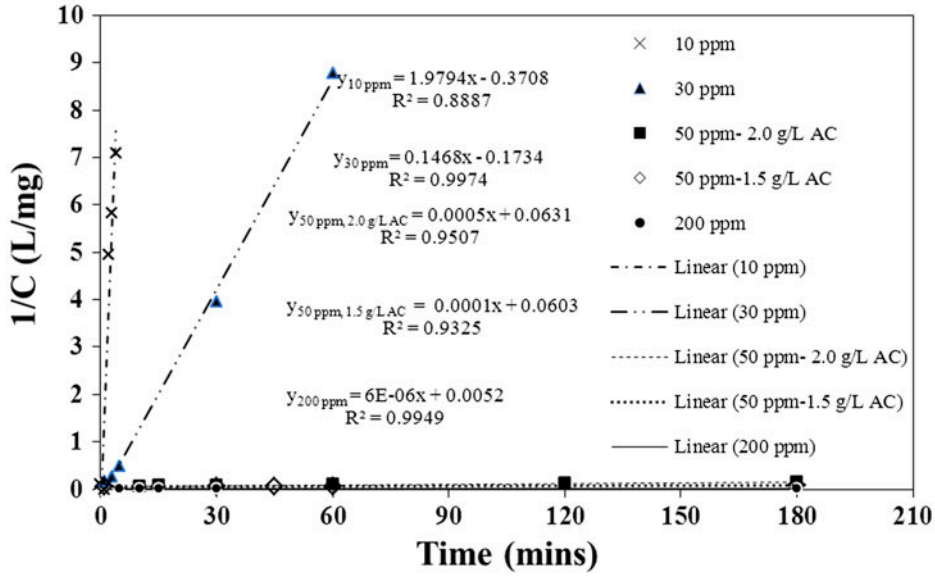

Fig. 4a. Second-order linear kinetic plot for the adsorption of rhodamine B under different conditions from synthetic wastewater using 2-g/L AC produced using phosphoric acid-based chemical activation of OFA waste (pH 3).

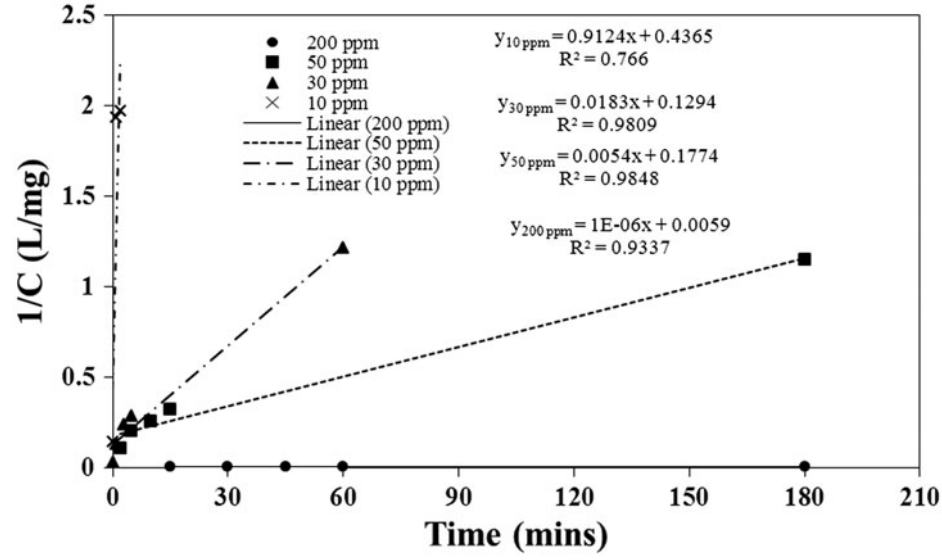

Fig. 4b. Second-order linear kinetic plot for the adsorption of different concentrations of MB from synthetic wastewater using 2-g/L AC produced using phosphoric acid-based chemical activation of OFA waste (pH 10).

maximum first-order rate constants of 0.0001 and 0.5661 min^{-1} were obtained for MB concentrations of 200 and 10 ppm, respectively. The second-order plots for MB adsorption are shown in Fig. 4b. A comparison of the second-order reaction rate constants at different concentrations shows a trend similar to that noted for RB. Furthermore, the second-order plots for the adsorption of MO onto the produced AC are shown in Fig. 4c, with the qualitative reaction rate constants trends similar to those noted for RB and MB. Higher reaction rate constants were observed for cationic dyes (MB and RB) compared to the anionic dye (MO). The difference in molecular structure of the dyes might explain the observed difference in their adsorption trends. Overall, the adsorption rate constant values for all dyes decrease with an increasing dye concentration

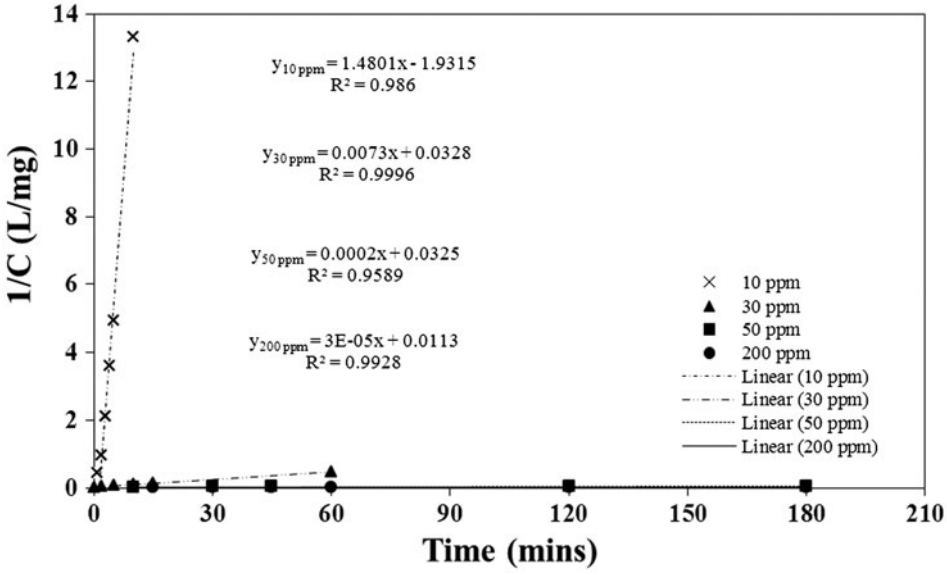

Fig. 4c. Second-order linear kinetic plot for the adsorption of different concentrations of MO from synthetic wastewater using 2-g/L AC produced using phosphoric acid-based chemical activation of OFA waste (pH 3).

for all three dyes. Despite the noted efficiency of AC for the removal of dyes, its surface sites are limited; therefore, an increase in the dye concentration will lead to the exhaustion of the limited number of sites, which will subsequently reduce the adsorptive removal of the dye. Similarly, an increase in the AC dosage will increase the number of sites available for adsorption, which will enhance the adsorptive removal of the dye. In general, a better fit is observed for the second-order kinetics compared to the first-order kinetics (Table 2).

3.4. Adsorption isotherm

Figs. 5a–5d show RB, MB, and MO adsorption-based removal vs. the amount of produced AC added. Fig. 5a shows that the adsorption of RB increases with an increase in AC dosage. The rate of the increase is more prominent at lower amounts of AC. Similar behavior is also observed in the MB and MO adsorption studies, as shown in Figs. 5b and 5c, respectively. Furthermore, Fig. 5d, which summarizes all these observations, shows that the produced AC is more effective at adsorbing the cationic dyes, RB and MB, than the anionic dye, MO. Significant adsorption of the cationic dyes is achieved at an AC dosage of 3.5 g/L. However, a higher dosage of produced AC is required for the near-complete adsorption of MO. The results were also fitted to Freundlich and Langmuir adsorption isotherms. Eqs. (1) and (2) represent the Freundlich isotherm and its linear form, respectively [17].

$$q_e = K_F C_e^{\frac{1}{n}} \tag{1}$$

$$\log q_e = \log K_F + \frac{1}{n} \log C_e \tag{2}$$

where q_e is the amount of adsorbed dye per gram of adsorbent, C_e is the equilibrium concentration of dye, and K_F and $1/n$ are the constants. The two constants, i.e. K_F and $1/n$, can be obtained from the plot of log (q_e) vs. log(C_e). The Langmuir isotherm and its linear form are presented in Eqs. (3) and (4), respectively [18]. The Langmuir constants, K_L and q_m, can be obtained from the plot of $1/q_e$ against $1/C_e$.

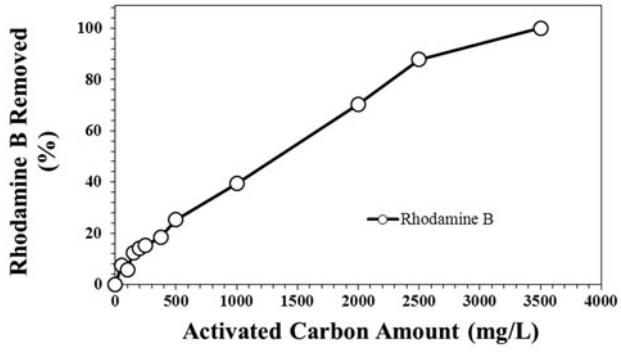

Fig. 5a. Effect of AC amount on the removal of rhodamine B from synthetic wastewater using AC produced using phosphoric acid-based chemical activation of OFA waste (rhodamine B = 100 ppm; solution pH 3).

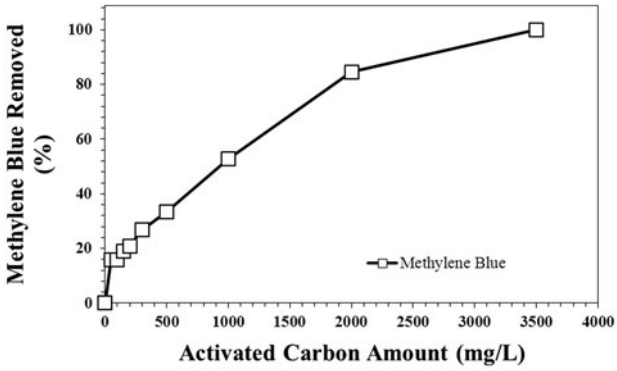

Fig. 5b. Effect of AC amount on the removal of MB from synthetic wastewater using AC produced using phosphoric acid-based chemical activation of OFA waste (MB = 100 ppm; solution pH 10).

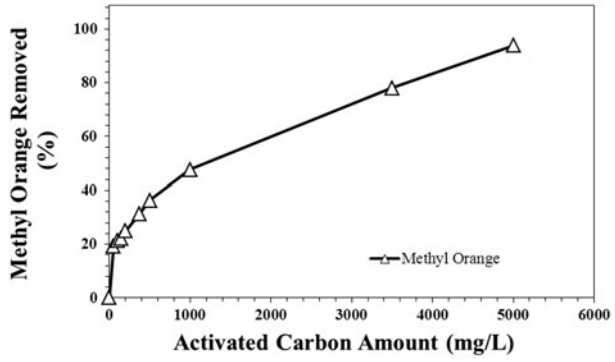

Fig. 5c. Effect of AC amount on the removal of MO from synthetic wastewater using AC produced using phosphoric acid-based chemical activation of OFA waste (MO = 100 ppm; solution pH 3).

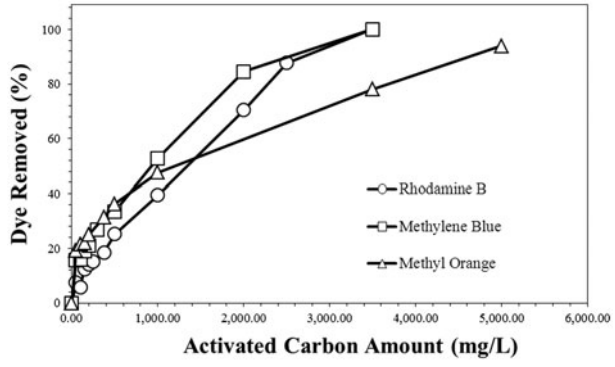

Fig. 5d. Effect of AC amount on the removal of different dyes from synthetic wastewater using AC produced using phosphoric acid-based chemical activation of OFA waste.

$$q_e = \frac{q_m K_L C_e}{1 + K_L C_e} \tag{3}$$

$$\frac{1}{q_e} = \left(\frac{1}{K_L q_m}\right)\frac{1}{C_e} + \frac{1}{q_m} \tag{4}$$

The Freundlich fit (Fig. 6) yields maximum and minimum K_F values of 3.5148 and 0.0013 L/g for MB and MO, respectively. This result also supports the aforementioned finding that the cationic dyes (MB and RB) adsorb better onto the produced AC compared to the anionic dye (MO). Furthermore, Fig. 7 shows the Langmuir model fit for the adsorption-based removal of RB, MB, and MO. Adsorption capacities of 540 and 104 mg/g were obtained for RB and MB, respectively. In general, the Freundlich isotherm model provides a better fit for the adsorption of MB and MO compared to the Langmuir adsorption isotherm model. Itodo

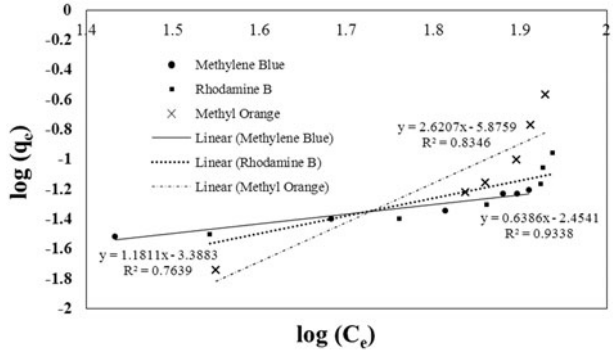

Fig. 6. Freundlich adsorption isotherm for the adsorption of different dyes from synthetic wastewater using AC produced using phosphoric acid-based chemical activation of OFA waste.

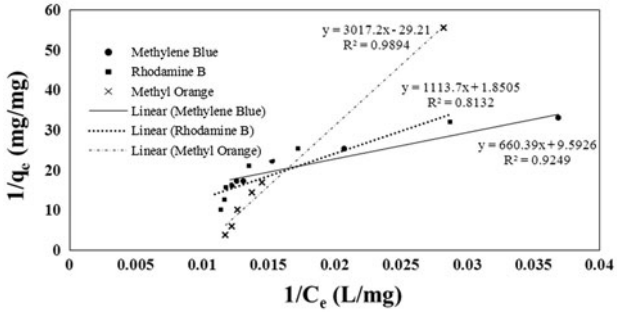

Fig. 7. Langmuir adsorption isotherm for the adsorption of different dyes from synthetic wastewater using AC produced using phosphoric acid-based chemical activation of OFA waste.

et al. noted the same results for the adsorption-based removal of MB [19]. Nevertheless, the Langmuir isotherm provided a better fit for RB compared to the Freundlich isotherm. The Freundlich and Langmuir constants for three dyes are provided in Table 3.

3.5. RSM modeling

The RSM, which is a widely used optimization method [20], was used to determine the importance of the pH, initial dye concentration, and amount of AC added on the dye adsorption. Considering the BBD, three levels were chosen for each of three independent variables, as indicated in Table 4, using the three levels of −1, 0, and +1 and equally spaced intervals [21]. The model equations for the adsorption-based removal of MB, RB, and MO in terms of the coded factors are given in Eqs. (5)–(7), respectively. The significance level of the models and model terms are provided in Table 5. Furthermore, Table 6 provides the salient characteristics of the models. The model outputs or response surface three-dimensional plots showing the effect of the above-mentioned three individual factors (i.e. pH, initial dye concentration, and amount of AC added) on the adsorption efficiency are presented in Figs. 8a–8c to 10a–10c, respectively.

$$\text{Amount of MB removed} = 71.8619 + 6.2325 \times A - 21.0814 \times B + 10.3303 \times C \quad (5)$$

$$\text{Amount of RB removed} = 53.7217 - 8.77099 \times A - 18.6747 \times B + 13.3694 \times C + 3.8417 \times AB - 6.1471 \times AC + 12.3741 \times B^2 \quad (6)$$

Table 3
Adsorption isotherm constants for Freundlich and Langmuir isotherms for the adsorption of RB, MB, and MO onto AC produced using phosphoric acid-based chemical activation of OFA waste (dye concentration = 100 ppm)

Parameter		n	K_F (L/g)	R^2
Freundlich isotherm	Methylene blue	1.5659	3.5148	0.9338
	Rhodamine *B*	0.8467	0.4090	0.7639
	Methyl orange	0.3816	0.0013	0.8346
Parameter		q_m (mg/g)	K_L (L/g)	R^2
Langmuir isotherm	Methylene blue	104.25	14.5257	0.9249
	Rhodamine *B*	540.39	1.6616	0.8132
	Methyl orange	−ve	−ve	0.9894

Table 4
RB, MB, and MO adsorption results for OFA-based AC, considering the Box–Behnken design

Run	*A*: pH	*B*: dye concentration (ppm)	*C*: AC concentration (ppm)	Rhodamine B amount removed (%)	Methylene blue amount removed (%)	Methyl orange amount removed (%)
1	10	100	2,000	52.8759	84.5409	45.7876
2	4	100	2,000	80.1693	68.5088	74.95
3	7	150	2,000	58.8494	64.8176	38.1218
4	10	50	1,500	71.3065	100	35.4087
5	7	100	1,500	56.3237	78.2865	43.0076
6	10	150	1,500	40.718	63.393	10.4176
7	4	150	1,500	53.1189	43.2981	44.3592
8	7	150	1,000	36.9985	45.9961	22.8537
9	7	50	1,000	68.7013	90.0211	51.2649
10	7	50	2,000	100	100	84.7905
11	4	50	1,500	99.0743	96.1349	69.812
12	4	100	1,000	40.9723	44.6697	48.3694
13	10	100	1,000	38.2675	54.538	12.7505

Table 5
Significant levels of the models and individual model terms at 5% ($p < 0.05$)

	Significance of model and model terms						
Response	Model	*A*	*B*	*C*	*AB*	*AC*	B^2
Rhodamine *B* amount removed (%)	<0.0001	0.0001	<0.0001	<0.0001	0.0315	0.0043	0.0002
Methylene blue amount removed (%)	0.0002	0.0664	<0.0001	0.0072	–	–	–
Methyl orange amount removed (%)	<0.0001	<0.0001	<0.0001	0.0002			

Table 6
Salient characteristics of RB, MB, and MO adsorption models developed using RSM methodology

Response	Response transformation	Adequate precision	R^2	Adjusted R^2	Predicted R^2	AAD (%)
Rhodamine *B* amount removed (%)	None	31.723	0.9918	0.9836	0.9617	3.10
Methylene blue amount removed (%)	None	13.413	0.8803	0.8404	0.7438	9.58
Methyl orange amount removed (%)	None	18.367	0.9397	0.9197	0.8675	11.54

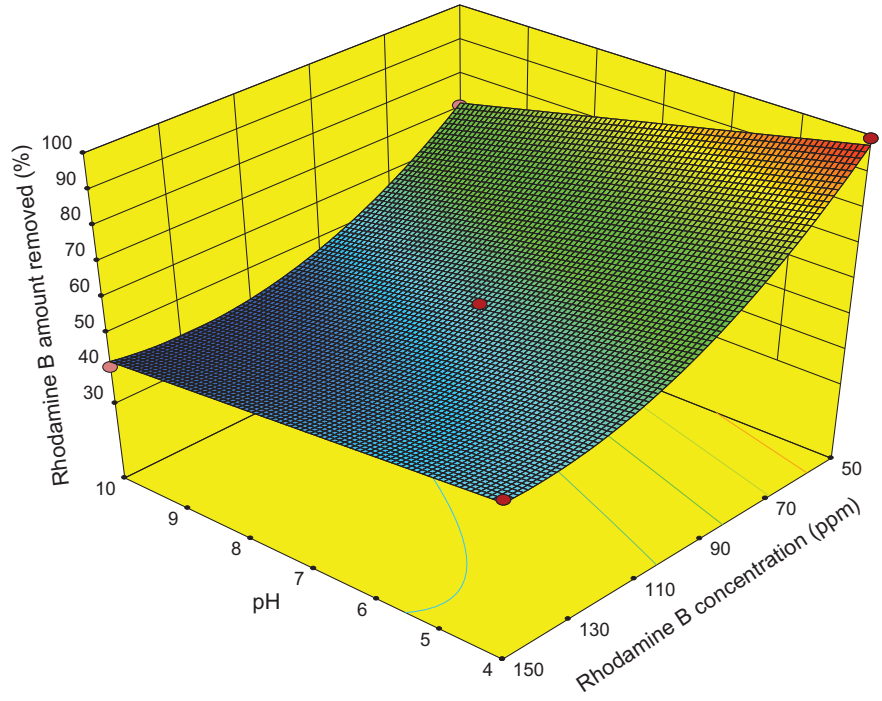

Fig. 8a. 3D graph showing the effects of pH and initial dye concentration on the removal of rhodamine B from synthetic wastewater using 1.5-g/L AC produced using phosphoric acid-based chemical activation of OFA waste.

$$\text{Amount of MO removed} = 44.7610 - 16.6408 \times A - 15.6905 \times B + 13.5514 \times C \quad (7)$$

where *A* denotes the pH (−1 = pH 4, 0 = pH 7, and +1 = pH 10), B denotes the initial dye concentration (−1 = 50 ppm, 0 = 100 ppm, and +1 = 150 ppm), and *C* denotes the amount of *AC* added (−1 = 1,000 ppm, 0 = 1,500 ppm, and +1 = 2,000 ppm). For all three

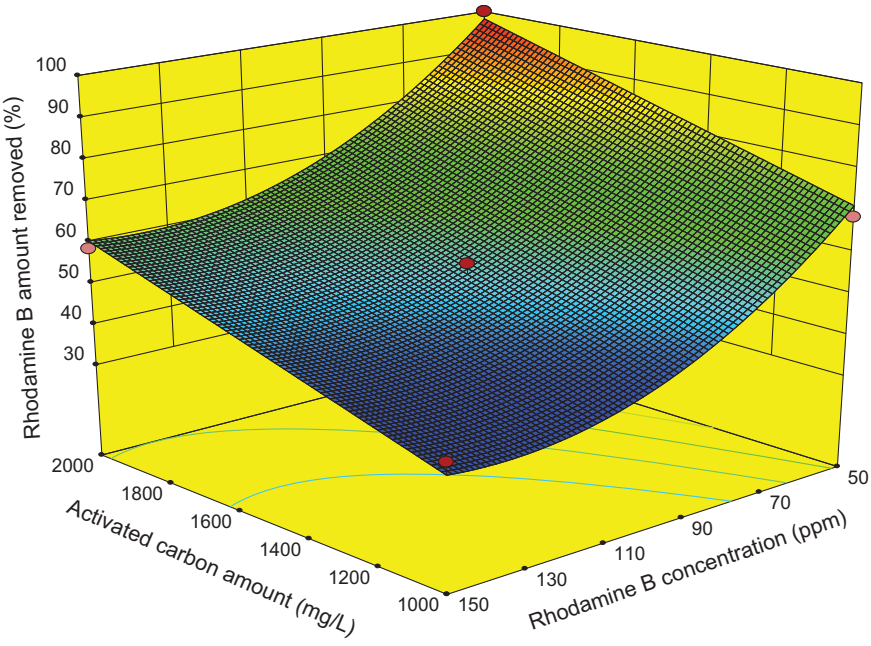

Fig. 8b. 3D graph showing the effects of initial AC and dye concentration on the removal of rhodamine B from synthetic wastewater using AC produced using phosphoric acid-based chemical activation of OFA waste (solution pH 7).

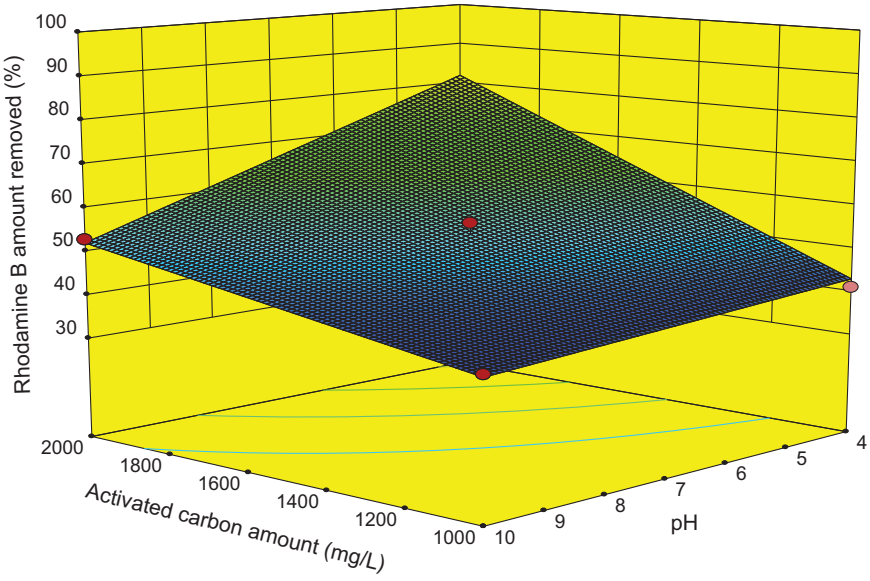

Fig. 8c. 3D graph showing the effects of pH and AC dosage on the removal of 100-ppm rhodamine B from synthetic wastewater using AC produced using phosphoric acid-based chemical activation of OFA waste.

models, only single factors and significant interaction effects based on a 5% level of significance are shown. From Eq. (5), the adsorption-based removal of MB increases with an increase in pH and OFA concentration but decreases with an increase in the initial MB concentration. As discussed earlier, the OFA-based AC utilized in this research has a pH_{zpc} of 5.6 (Fig. 2c). Therefore, below pH 5.6, the AC will be predominantly positively charged, and thus, an electrostatic repulsion will exist between the AC and the positive dye. However, above pH 5.6, the surface of the AC will be predominantly negatively charged,

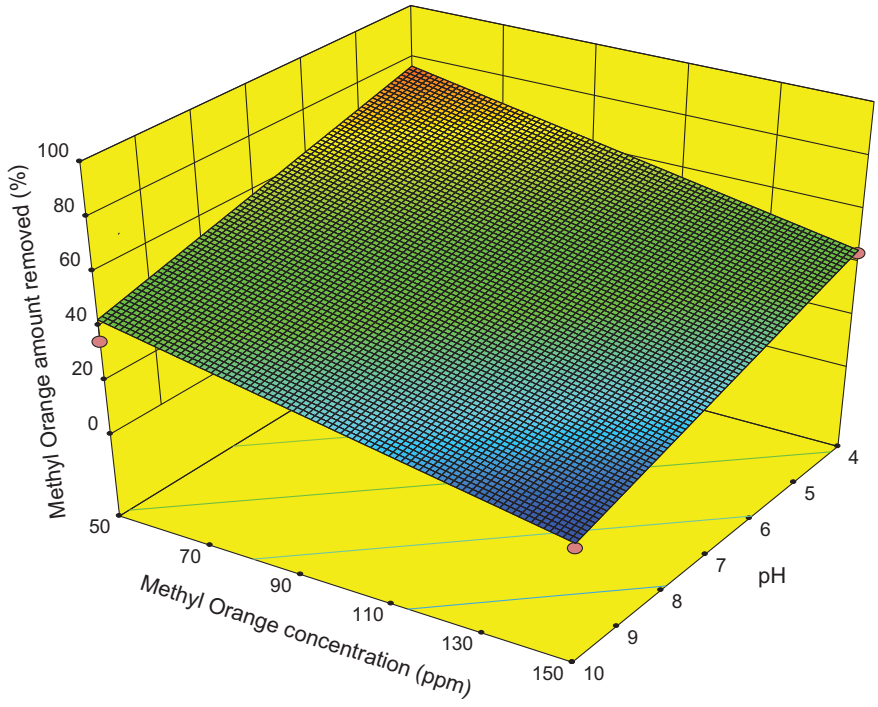

Fig. 9a. 3D graph showing the effects of pH and initial dye concentration on the removal of MO from synthetic wastewater using 1.5-g/L AC produced using phosphoric acid-based chemical activation of OFA waste.

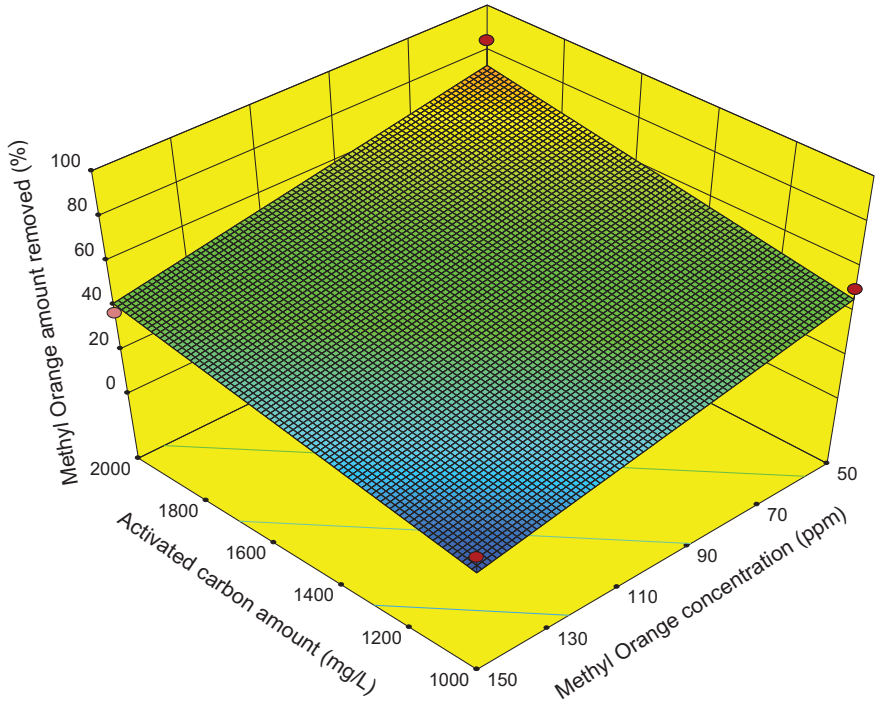

Fig. 9b. 3D graph showing the effects of initial AC amount and dye concentration on the removal of MO from synthetic wastewater using AC produced using phosphoric acid-based chemical activation of OFA waste (solution pH 7).

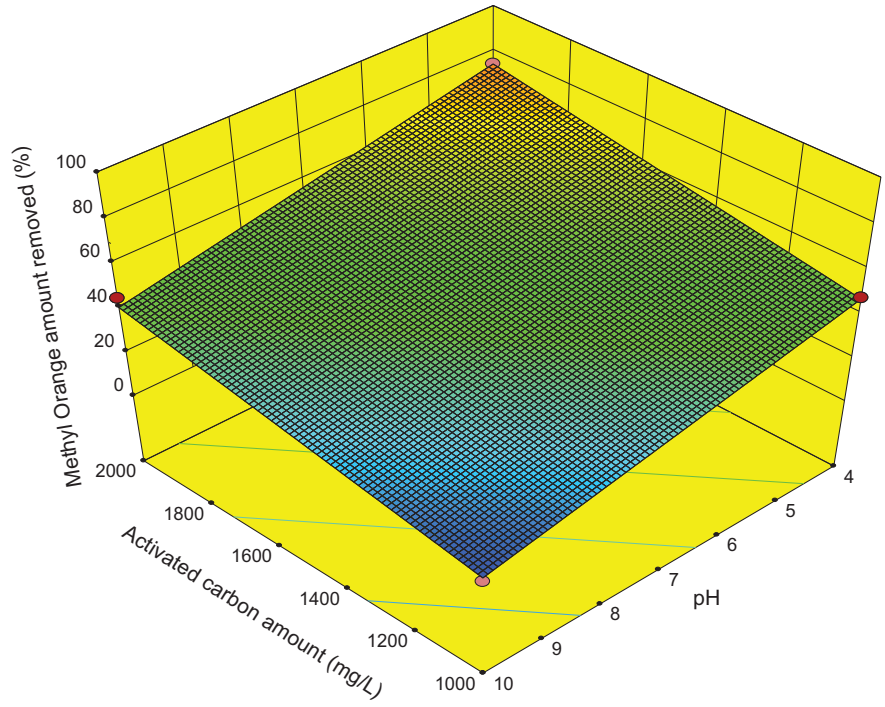

Fig. 9c. 3D graph showing the effects of pH and AC amount on the removal of 100-ppm MO from synthetic wastewater using AC produced using phosphoric acid-based chemical activation of OFA waste.

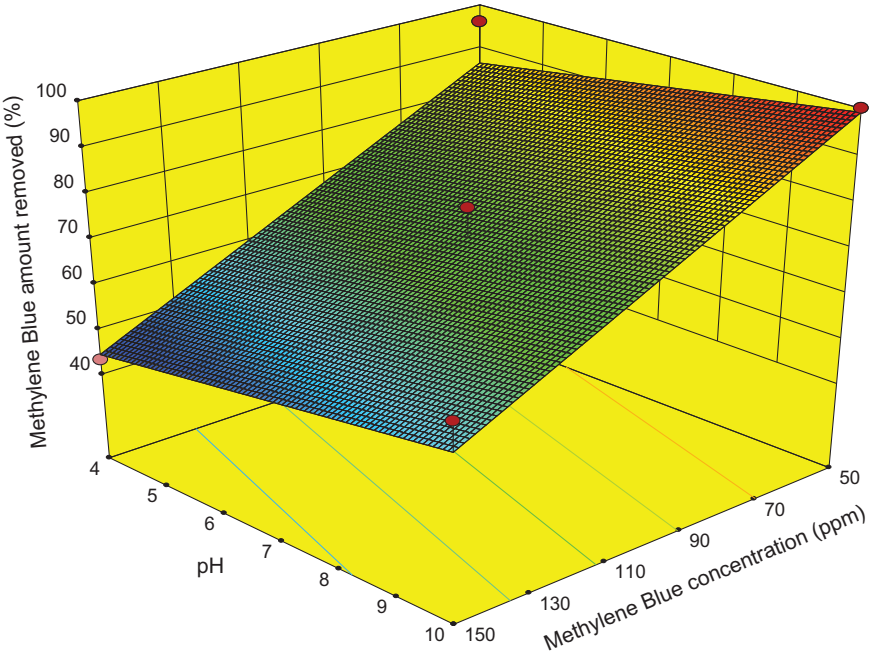

Fig. 10a. 3D graph showing the effects of pH and initial dye concentration on the removal of MB from synthetic wastewater using AC produced using phosphoric acid-based chemical activation of OFA waste (OFA dosage = 1.5 g/L).

which will cause an electrostatic attraction between the positive dye and negative AC. Furthermore, despite the noted efficiency of AC for the removal of the dyes, its surface sites are limited. Therefore, an increase in dye concentration will lead to the exhaustion of the limited sites, which will subsequently

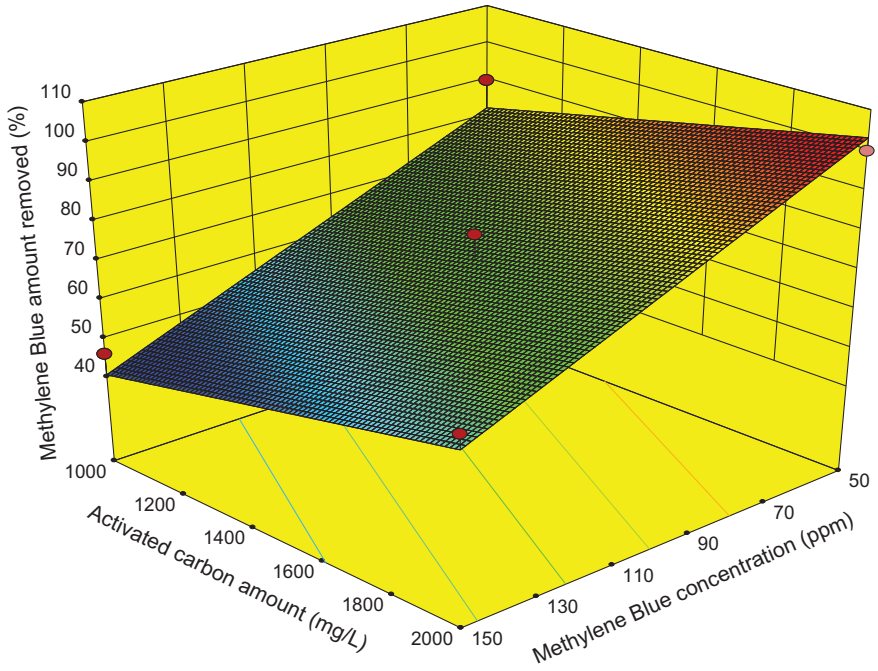

Fig. 10b. 3D graph showing the effects of initial dye concentration and AC amount on the removal of MB from synthetic wastewater using AC produced using phosphoric acid-based chemical activation of OFA waste (initial dye concentration = 100 ppm).

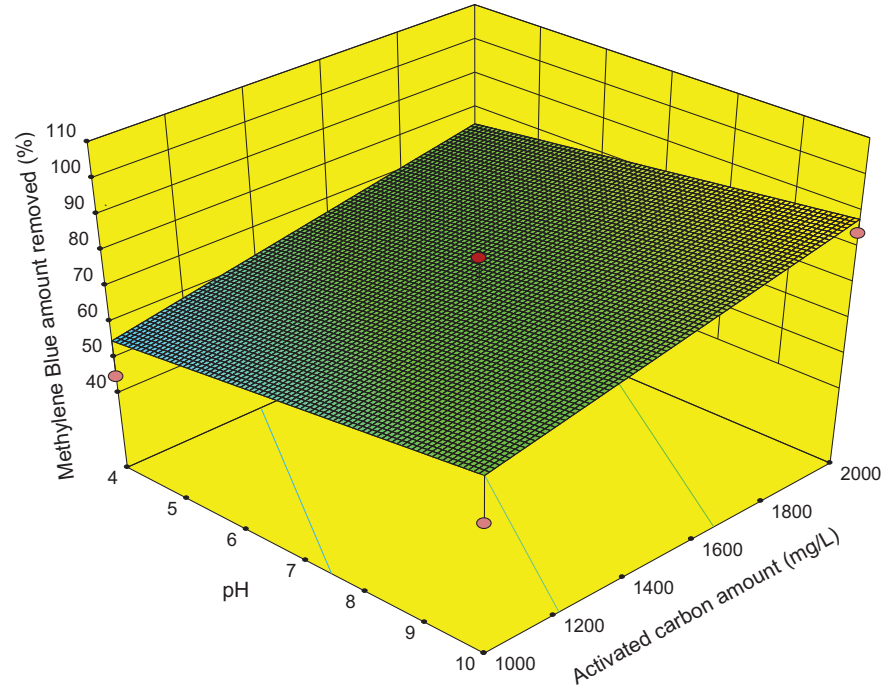

Fig. 10c. 3D graph showing the effects of pH and AC amount on the removal of MB from synthetic wastewater using AC produced using phosphoric acid-based chemical activation of OFA waste (solution pH 7).

reduce the adsorptive removal of the dye. Similarly, an increase in the AC dosage will increase the number of sites available for adsorption, which will enhance the adsorptive removal of the dye. The absolute values of the coefficient factors are in the following order: MB concentration > AC added > pH; in other words, the MB concentration has a greater impact on the model developed, whereas pH has the smallest impact. From Table 5, only pH is not a significant factor of the model developed based on a 95% confidence interval. This result occurs because the adsorption of MB shows a changing trend vs. pH. As shown in Section 3.2, the adsorption of MB decreases with an increase in pH until approximately 5, with an increased adsorption for higher pH values. A reasonable fit was obtained for the experimental data for extracting an adequate precision value and an average absolute deviation (AAD) value. The adequate precision value measures the signal-to-noise ratio, with a value greater than 4 being desirable. An adequate precision value of 13.4 was obtained for MB. Furthermore, the AAD, which is a measure of the prediction capability of the model (e.g. adsorption, in the present case) is calculated using Eq. (8) [22]. The AAD should be as low as possible.

$$\mathrm{AAD} = \sum_{i=1}^{p} \left(\frac{|y_{i,\mathrm{exp}} - y_{i,\mathrm{cal}}|}{y_{i,\mathrm{exp}}} \right) / p \times 100 \tag{8}$$

where $y_{i,\mathrm{exp}}$ and $y_{i,\mathrm{cal}}$ are the experimental and calculated responses, respectively, and p is the number of the experimental run. An AAD of 9.58% was obtained for the MB model. The adjusted R^2 and predicted R^2 are considered to be in reasonable agreement if their difference is less than 0.2. For the MB model, the difference between the adjusted R^2 and predicted R^2 is only 0.0966, which shows that they are in reasonable agreement. From Eq. (6), the relative impact of the above-mentioned modeling factors on the removal of RB is similar to that of MB. However, the relative impact of the modeling factors on the adsorption of MO (Eq. (7)) follows the following order: pH > AC added > MO concentration. Overall, an excellent fit was obtained for the RB model, with R^2, adequate precision, and AAD values of 0.9918, 31.723, and 3.10%, respectively. A very good fit was obtained for the MO model, with R^2, adequate precision, and AAD values of 0.9397, 18.367, and 11.54%, respectively. The difference between the adjusted R^2 and predicted R^2 for the RB and MO models are 0.0219 and 0.0522, respectively, which shows that they are in reasonable agreement. Overall, the RSM models and outcomes shown in Figs. 8a–8c to 10a–10c indicate that the RSM approach can be used to predict the removal of RB, MB, and MO from the aqueous phase using OFA-based AC under a varying set of operational conditions.

4. Conclusions

We studied the conversion of heavy OFA into AC and its application to the adsorption-based removal of RB, MB, and MO from the aqueous phase. The conclusions of this research are as follows:

(1) An optimum form of AC was produced with a SSA_{BET} value of 63 m^2/g for a phosphoric acid strength of 40% (w/w %), an impregnation ratio R of 0.8 (mL-acid/gm-fly ash), and a furnace temperature of 500°C (for 2 h).
(2) The optimum adsorption of RB was achieved at pH 4; the adsorption decreased with a further increase in pH. Both, a shift in the AC surface charge and speciation of the RB carboxylic group to an anionic species, caused the reduced adsorption of RB at higher pH.
(3) Increased MB adsorption was observed at pH 5 and above due to the cationic nature of the dye and the increased negative AC surface change.
(4) The observed decrease in MO adsorption with an increase in pH was due to increased presence of negative charge on the AC surface, resulting in electrostatic repulsion with the MO sulfonate group.
(5) Kinetics studies showed that the second-order rate constant values are higher at lower dye concentrations due to the comparatively higher availability of active surface sites.
(6) The Freundlich isotherm model provided a better fit for the adsorption of MB and MO, whereas the Langmuir model provided a better fit for RB adsorption.
(7) The relative impact of the adsorption variables on the RSM-based models was found to follow the following order: initial dye concentration > AC amount > pH for cationic dyes and pH > AC amount > initial dye concentration for MO.

Acknowledgments

The authors thank KACST for providing the research grant for this work through NSTIP project #11-ENV2142-04. The authors also thank the Civil and Environmental Engineering Department and Deanship of Research at KFUPM for its support.

References

[1] B.H. Hameed, A.L. Ahmad, K.N.A. Latiff, Adsorption of basic dye (methylene blue) onto activated carbon prepared from rattan sawdust, Dyes Pigm. 75 (2007) 143–149.

[2] A.M. Talarposhti, T. Donnelly, G.K. Anderson, Colour removal from a simulated dye wastewater using a two-phase anaerobic packed bed reactor, Water Res. 35 (2001) 425–432.

[3] A. Kechi, R.B. Chavan, R. Moeckel, Ethiopian dye plants as a source of natural dyes for cotton dyeing, Univers. J. Environ. Res. Technol. 3 (2013) 501–510.

[4] N. Mathur, P. Bhatnagar, P. Nagar, M.K. Bijarnia, Mutagenicity assessment of effluents from textile/dye industries of Sanganer, Jaipur (India): A case study, Ecotox. Environ. Saf. 61 (2005) 105–113.

[5] S. Wang, M. Soudi, L. LI, Z.H. Zhu, Coal ash conversion into effective adsorbents for removal of heavy metals and dyes from wastewater, J. Hazard. Mater. 133 (2006) 243–251.

[6] G. Annadurai, R.-S. Juang, D.-J. Lee, Use of cellulose-based wastes for adsorption of dyes from aqueous solutions, J. Hazard. Mater. 92 (2002) 263–274.

[7] M. Ahmaruzzaman, A review on the utilization of fly ash, Prog. Energy Combust. 36 (2010) 327–363.

[8] S. Wang, H. Wu, Environmental-benign utilisation of fly ash as low-cost adsorbents, J. Hazard. Mater. 136 (2006) 482–501.

[9] K. Rastogi, J.N. Sahu, B.C. Meikap, M.N. Biswas, Removal of methylene blue from wastewater using fly ash as an adsorbent by hydrocyclone, J. Hazard. Mater. 158 (2008) 531–540.

[10] D. Mohan, K.P. Singh, G. Singh, K. Kumar, Removal of dyes from wastewater using flyash, a low-cost adsorbent, Ind. Eng. Chem. 41 (2002) 3688–3695.

[11] M. Visa, C. Bogatu, A. Duta, Simultaneous adsorption of dyes and heavy metals from multicomponent solutions using fly ash, Appl. Surf. Sci. 256 (2010) 5486–5491.

[12] S. Andini, R. Cioffi, F. Colangelo, F. Montagnaro, L. Santoro, Adsorption of chlorophenol, chloroaniline and methylene blue on fuel oil fly ash, J. Hazard. Mater. 157 (2008) 599–604.

[13] S.L.C. Ferreira, R.E. Bruns, H.S. Ferreira, G.D. Matos, J.M. David, G.C. Brandão, E.G.P. da Silva, L.A. Portugal, P.S. dos Reis, A.S. Souza, W.N.L. dos Santos, Box–Behnken design: An alternative for the optimization of analytical methods, Anal. Chim. Acta 597 (2007) 179–186.

[14] Y. Guo, J. Zhao, H. Zhang, S. Yang, J. Qi, Z. Wang, H. Xu, Use of rice husk-based porous carbon for adsorption of Rhodamine B from aqueous solutions, Dyes Pigm. 66 (2005) 123–128.

[15] F. Liu, S. Teng, R. Song, S. Wang, Adsorption of methylene blue on anaerobic granular sludge: Effect of functional groups, Desalination 263 (2010) 11–17.

[16] A.K. Bhattacharya, T.K. Naiya, S.N. Mandal, S.K. Das, Adsorption, kinetics and equilibrium studies on removal of Cr(VI) from aqueous solutions using different low-cost adsorbents, Chem. Eng. J. 137 (2008) 529–541.

[17] G. Limousin, J.P. Gaudet, L. Charlet, S. Szenknect, V. Barthès, M. Krimissa, Sorption isotherms: A review on physical bases, modeling and measurement, Appl. Geochem. 22 (2007) 249–275.

[18] Y.-S. Ho, Selection of optimum sorption isotherm, Carbon 42 (2004) 2115–2116.

[19] A.U. Itodo, H.U. Itodo, M.K. Gafar, Estimation of specific surface area using Langmuir isotherm method, J. Appl. Sci. Environ. Manage. 14 (2010) 141–145.

[20] D. Baş, İ.H. Boyacı, Modeling and optimization I: Usability of response surface methodology, J. Food Eng. 78 (2007) 836–845.

[21] M.A. Bezerra, R.E. Santelli, E.P. Oliveira, L.S. Villar, L.A. Escaleira, Response surface methodology (RSM) as a tool for optimization in analytical chemistry, Talanta 76 (2008) 965–977.

[22] D. Baş, İ.H. Boyacı, Modeling and optimization II: Comparison of estimation capabilities of response surface methodology with artificial neural networks in a biochemical reaction, J. Food Eng. 78 (2007) 846–854.